Review

Recent Advances in Nitrate Reduction Electrolyzers for Sustainable Ammonia Synthesis

Keon-Han Kim and Jeonghoon Lim *

Posted Date: 22 January 2025

doi: 10.20944/preprints202501.1574.v1

Keywords: nitrate reduction; ammonia synthesis; electrocatalysis; sustainable nitrogen cycling; electrolyzer design; catalyst engineering; membrane electrode assembly (MEA)

 doi:10.20944/preprints202501.1574.v1

Review

Recent Advances in Nitrate Reduction Electrolyzers for Sustainable Ammonia Synthesis

Keon-Han Kim [1,3,4], and Jeonghoon Lim [2,3,*]

[1] Chemical Science Division, Lawrence Berkeley National Laboratory, Berkeley, California 94720, USA; keonhankim89@gmail.com

[2] Energy Storage and Distributed Resources Division, Lawrence Berkeley National Laboratory, Berkeley, California 94720, USA

[3] Department of Chemical and Biomolecular Engineering, University of California, Berkeley, CA 94720, USA

[4] Research Institute of Basic Science, Seoul National University, Seoul 08826, Republic of Korea

* Correspondence: jeonghoonlim@lbl.gov or jeonghoon.lim20@gmail.com

Abstract: The electrochemical reduction of nitrate (NO_3RR) to ammonia (NH_3) provides a decentralized and environmentally friendly route for sustainable ammonia production while addressing the urgent issue of nitrate pollution in water bodies. Recent advancements in NO_3RR research have improved catalyst design, mechanistic understanding, and electrolyzer technology, enhancing selectivity, yield, and energy efficiency. This review explores cutting-edge developments, focusing innovative designs of catalyst and electrolyzer such as membrane electrode assemblies (MEA) and electrolyzer configuration, understanding the role of membranes in MEA designs, and various types of hybrid reactors, and membrane-free reactors. Furthermore, the integration of NO_3RR with anodic oxidation reactions has been demonstrated to improve overall efficiency by generating valuable co-products. However, challenges such as competitive hydrogen evolution, catalyst degradation, and scalability remain critical barriers to large-scale adoption. We provide a comprehensive overview of recent progress, evaluates current limitations, and identifies future research directions for realizing the full potential of NO_3RR in sustainable nitrogen cycling and ammonia synthesis.

Keywords: nitrate reduction; ammonia synthesis; electrocatalysis; sustainable nitrogen cycling; electrolyzer design; catalyst engineering; membrane electrode assembly (MEA)

1. Introduction

Ammonia is a cornerstone of modern agriculture and industrial processes, with its demand continually increasing to meet the needs of a growing global population. Conventionally, ammonia is synthesized through the Haber-Bosch process, which, while highly effective, is energy-intensive, consuming approximately 1-2% of the world's total energy supply, and is a major contributor to greenhouse gas emissions.[1-7] Simultaneously, nitrate pollution from agricultural runoff and industrial effluents has become a critical environmental challenge, leading to eutrophication and water quality degradation.[8,9] Addressing these concurrent issues requires innovative approaches that are both environmentally sustainable and economically viable.

The Haber-Bosch process, despite its efficiency, relies heavily on fossil fuels, emitting substantial amounts of CO_2 and creating an urgent need for alternative synthesis methods. On the other hand, nitrate pollution, often stemming from agricultural fertilizers and industrial discharge, exacerbates environmental issues such as algal blooms and biodiversity loss.[10] These interlinked challenges highlight the necessity of integrating sustainable practices into nitrogen management systems.[11]

Electrochemical nitrate reduction (NO_3RR) to ammonia has emerged as a transformative solution, offering a decentralized, low-energy pathway for ammonia production while simultaneously mitigating nitrate contamination in water.[12-20] This method leverages

 doi:10.20944/preprints202501.1574.v1

advancements in electrochemical technologies to directly address both ammonia demand and environmental remediation. Unlike the Haber-Bosch process, NO_3RR operates under ambient conditions, utilizing renewable electricity and water as primary inputs, thereby significantly reducing energy consumption and greenhouse gas emissions.[21,22]

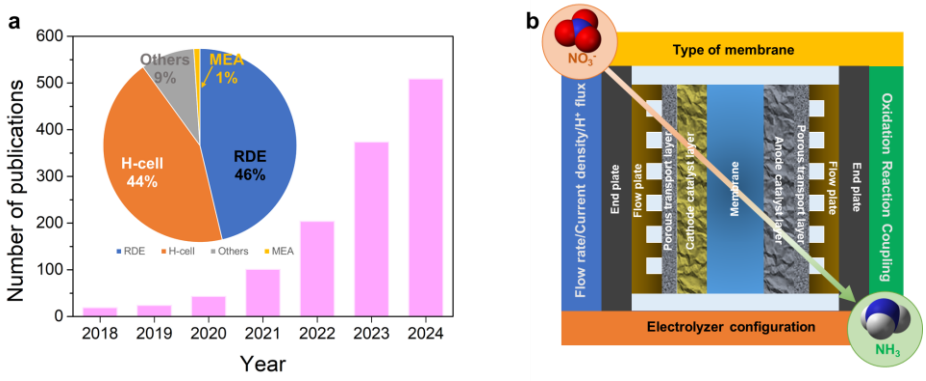

Figure 1. (a) Distribution and annual trend of publications on electrochemical nitrate reduction from 2018 to 2024. The pie chart shows the proportion of research using different experimental cell configurations, including rotating disk electrodes (RDE, 46%), H-cells (44%), membrane electrode assemblies (MEA, 1%), and others (9%). **(b)** Schematic representation of critical parameters influencing nitrate reduction in electrochemical systems, including membrane type, flow rate/current density, H^+ flux, electrolyzer configuration, and the coupling of oxidation and reduction reactions for ammonia (NH_3) production.

The trends in nitrate reduction research over recent years indicate a growing interest in understanding and optimizing electrochemical systems for sustainable ammonia production. A significant proportion of studies have utilized rotating disk electrodes (RDE, 46%) and H-cells (44%), with a marked increase in publications from 2018 to 2024 (**Figure 1a**). RDE and H-cells configurations have been instrumental in elucidating reaction mechanisms and evaluating catalyst performance. However, it is notable that only 1% of studies have employed membrane electrode assemblies (MEA), highlighting their limited exploration in this field despite their critical importance for scalability. MEA-based systems are essential for the transition of nitrate reduction technologies from laboratory-scale research to industrial applications. As research increasingly focuses on achieving practical, scalable solutions, the development and optimization of MEA systems will be paramount. We further illustrate the key factors influencing nitrate reduction, including membrane type, flow conditions, and reaction coupling, which must be systematically addressed to enable efficient and sustainable industrial processes (**Figure 1b**).

The core of NO_3RR research revolves around two major pillars: catalyst innovation and electrolyzer design. Catalysts are the driving force of nitrate conversion, with materials such as heterostructured catalysts and single-atom catalysts (SACs) enabling precise control over reaction pathways.[23-27] Heterostructured catalysts leverage synergistic effects between different materials, achieving exceptional Faradaic efficiencies (FE) and stability under industrial conditions.[28-31] SACs, on the other hand, provide unparalleled site-specific activity, allowing for enhanced selectivity and reduced side reactions. Recent studies have also explored the potential of cascade catalysis within yolk-shell nanostructures,[32,33] which offer spatial separation of reaction intermediates, further optimizing nitrate-to-ammonia conversion.

Complementing these advancements in catalysts are innovations in electrolyzer configurations. Proton exchange membrane electrode assemblies (PEMEAs) represent a significant leap forward, offering "zero-gap" cell designs that minimize Ohmic losses and enhance ionic transport.[34-36] Such designs have demonstrated nearly complete nitrate-to-ammonia conversion in industrial applications, underscoring their scalability and economic feasibility. In parallel, novel configurations such as membrane-free reactors and hybrid systems have expanded the operational flexibility of NO_3RR technologies, addressing challenges related to system stability and product selectivity.[37-39] Beyond these innovations, there is a growing emphasis on understanding the fundamental

 doi:10.20944/preprints202501.1574.v1

mechanisms underlying NO_3RR. Mechanistic studies provide insights into the stepwise reduction of nitrate to ammonia, identifying key intermediates and reaction bottlenecks.[40,41] This knowledge has informed the development of advanced catalysts and reactor designs, enabling researchers to fine-tune systems for maximum efficiency and selectivity.[42,43] For example, computational modeling of SAC has revealed the importance of electronic interactions between catalytic sites, guiding the synthesis of more effective materials.[44] Furthermore, the integration of NO_3RR with wastewater treatment processes offers practical solutions for simultaneous nitrate removal and ammonia production.[45-47] Industrial and agricultural waste streams, rich in nitrate pollutants, can serve as feedstocks for ammonia production, transforming a waste management challenge into a resource recovery opportunity.[48] MEA and membrane-free reactors have shown particular promise in this context, offering robust performance under real-world conditions and meeting stringent regulatory standards for effluent quality.[38,49] The environmental benefits of NO_3RR extend beyond greenhouse gas reduction and nitrate remediation.[40] By decentralizing ammonia production, NO_3RR systems can reduce reliance on large-scale industrial facilities, enabling localized and on-demand ammonia generation.[37,45,50,51] This shift has the potential to enhance food security in remote and underserved regions, where access to synthetic fertilizers is limited.[52,53]

This review provides a detailed examination of recent advancements in NO_3RR, exploring the interplay between material properties, reaction mechanisms, and system-level innovations. By addressing the current challenges and highlighting promising strategies, we aim to provide a comprehensive perspective on the future of NO_3RR in achieving sustainable ammonia synthesis. Through this lens, we hope to inspire further research and development efforts aimed at bridging the gap between laboratory-scale success and real-world implementation, ultimately contributing to global sustainability goals.

2. Catalyst Innovations in MEA Systems

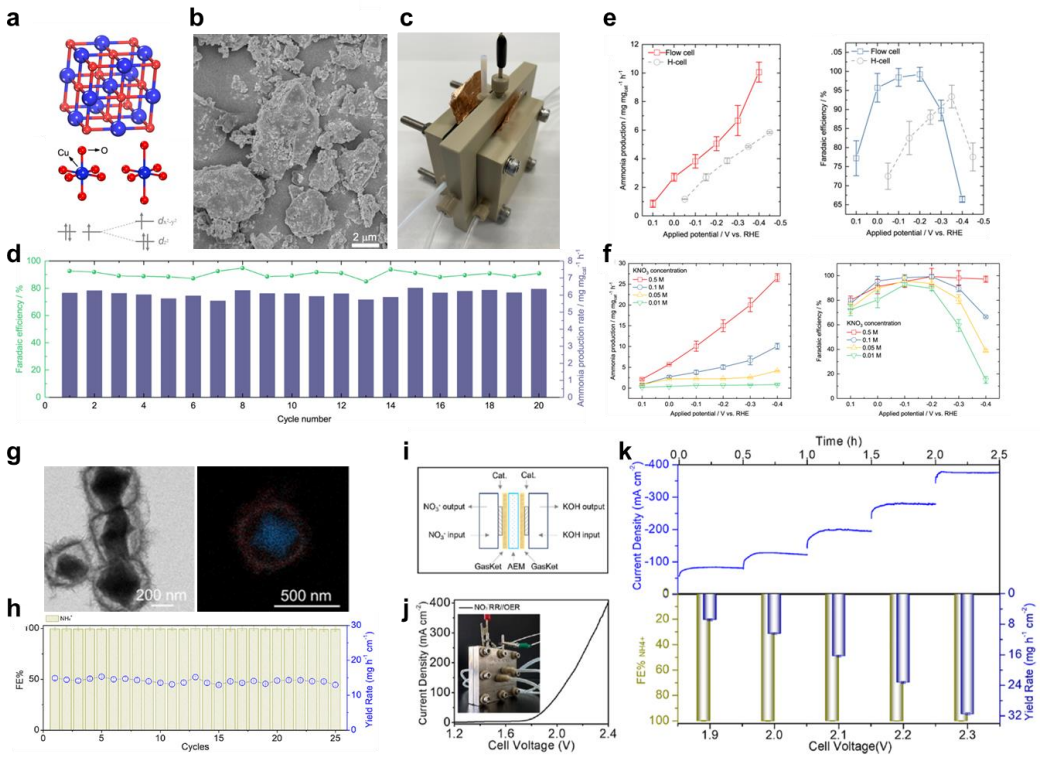

Figure 2. **(a)** A schematic representation of rock-salt structure, **(b)** SEM image of $Mg_{0.2}Co_{0.2}Ni_{0.2}Cu_{0.2}Zn_{0.2}O$ (RS-20), **(c)** Flow cell setup, **(d)** Electrochemical nitrate reduction of RS-20, **(e)** Ammonia production and FE with 1M KOH and **(f)** Diverse nitrate concentrion in the flow cell. **(g)** TEM image and EDS elemental mapping images of Cu2O@CoO yolk−shell nanocubes, **(h)** Continuous cycling tests at −0.8 V versus RHE were performed on Cu_2O@CoO yolk-shell nanocubes, evaluating the corresponding NH_4^+ FE and production rate. Electrochemical performance of the MEA system: **(i)** A schematic illustration of the MEA nitrate electrolysis cell setup. **(j)**

 doi:10.20944/preprints202501.1574.v1

Polarization curve of the MEA nitrate electrolysis cell featuring a Cu_2O@CoO yolk-shell nanocube cathode and an IrO_2 anode, with an inset displaying a photograph of the MEA cell. **(k)** Current–time (i–t) curves of the MEA nitrate electrolysis cell using the Cu_2O@CoO yolk-shell nanocube cathode and IrO_2 anode, measured within a cell voltage range of 1.9–2.3 V, along with the corresponding NH_4^+ FE and production rate. Reproduced with permission from Ref. [54] and Ref. [55], Copyright (2024), Springer Nature and American Chemical Society.

2.1. Heterostructured Catalysts

Heterostructured catalysts have captured significant attention in the realm of sustainable ammonia production due to their ability to integrate multiple functionalities into a single framework, thereby enhancing overall catalytic performance.[56-60] A prime example of this is Cu-Ni phosphide catalysts, which possess a unique structural composition that promotes efficient charge transfer while stabilizing critical reaction intermediates during the electrochemical NO_3RR process. These innovations have resulted in impressive metrics, achieving over 90% FE for NO_3RR reactions.[61-66] S. Sun et al. investigated a Cu-Co synergistic effect has shown excellent performance in ammonia production, particularly in high-entropy oxides. Using $Mg_{0.2}Co_{0.2}Ni_{0.2}Cu_{0.2}Zn_{0.2}O$ (RS-20), it was found that high-spin Co states are critical for enhancing the Cu-Co synergy, facilitating efficient ammonia generation (**Figure 2a-f**).[54] In contrast, Li incorporation reduced performance by inducing low-spin Co states, diminishing the synergistic effect. These findings highlight the role of spin states and magnetic effects in optimizing catalytic selectivity for ammonia synthesis, bridging insights between electrocatalysis and thermal catalysis. Z. Ma et al. explored the multi-electron/proton transfer process and reliance on atomic H* generated from water splitting pose challenges, necessitating efficient catalysts. In this study, three-dimensional (3D) porous phosphorus (P)-doped Cu–Ni alloy catalysts were developed via one-step electrodeposition.[63] The 3D porous structure enhances hydrophilicity and active site density, while Ni alloying tunes the Cu d-band center, optimizing intermediate adsorption. P-doping facilitates hydrogenation by promoting atomic H* generation and accelerating the reaction rate. Density functional theory (DFT) calculations reveal charge transfer between $P^{\delta-}$, $Ni^{\delta+}$, and $Cu^{\delta+}$, enhancing atomic H* availability and catalytic activity at low overpotentials. The catalyst achieved a remarkable ammonia yield rate of 848.1 $\mu mol \cdot h^{-1} \cdot cm^{-2}$ and a FE of 96.1%, demonstrating an effective strategy for NRA catalyst design through atomic H* reduction enhancement. S. Lv et al. reported Ni_2P@Cu_3P catalyst was in situ fabricated on copper foam, achieving exceptional NRA performance.[64] The interface coupling between Ni_2P and Cu_3P optimized the surface electronic structure, exposing more metal-P bonds and enhancing catalytic activity. The catalyst exhibited a remarkable NH_3 FE of 96.97%, a yield rate of 0.2784 $mmol \cdot h^{-1} \cdot cm^{-2}$, a selectivity rate of 98.07%, and a NO_3^- conversion rate of 99.35%. Density functional theory (DFT) calculations revealed that interface electron coupling regulated the adsorption energies of intermediates, improving catalytic efficiency. This study offers valuable insights into designing efficient electrocatalysts for nitrate-to-ammonia conversion. M. Jin et al. exhibited the synthesis of heterostructure copper-nickel phosphide (Cu_3P–Ni_2P) electrocatalysts using a vapor-phase hydrothermal method and evaluates their performance in electrocatalytic NO_3RR to ammonia across three electrochemical reactor types.[65] Detailed investigations in H-type cells, rotating disk electrodes, and membrane-electrode-assemblies (MEA) revealed that Cu_3P–Ni_2P/CP–0.5 achieved an exceptional ammonia yield rate of 1.9 $mmol \cdot h^{-1} \cdot cm^{-2}$ in an MEA system with an anion exchange membrane, outperforming most reported catalysts. Theoretical calculations and in-situ spectroscopy confirmed that the heterointerface in Cu_3P–Ni_2P/CP enhances nitrate adsorption, activation, and conversion via a hydrodeoxygenation pathway, offering insights into designing advanced electrocatalysts for NO_3RR. L. Min et al. designed a Cu@Ni_2P-NF metal-semiconductor heterostructure to enhance NO_3-RR performance through Schottky contacts, which optimize H* adsorption and boost NO_3^- adsorption via interfacial electron transfer.[66] The synergistic effects from the built-in electric field significantly improve catalytic activity, achieving an ammonia yield of 0.374 $mmol \cdot h^{-1} \cdot cm^{-2}$ at −0.2 V (vs. RHE), a nitrate removal efficiency of 94.63%, and a selectivity of 90.25% in 1 M KOH with 20 mM KNO_3. Additionally, a Zn-NO_3^- battery demonstrates energy conversion with a power density of 5.09 $mW \cdot cm^{-2}$. This work highlights the potential of Schottky heterojunction design for developing advanced NO_3RR electrocatalysts. Mechanistic insights reveal

 doi:10.20944/preprints202501.1574.v1

that copper sites play a vital role in activating nitrate molecules. These sites facilitate the initial steps of the reduction process. Concurrently, nickel sites are pivotal in assisting the hydrogenation of intermediate species, leading to a significant enhancement in the kinetics of the overall reaction. The synergistic interplay between these two elements not only boosts efficiency but also stabilizes the reaction pathways involved. Furthermore, recent experimental studies have validated the industrial viability of these heterostructured catalysts, with ammonia yield rates exceeding 1.6 $mmol \cdot h^{-1} \cdot cm^{-2}$ when deployed in proton exchange membrane electrolysis (PEMEA) systems.[67] This performance underscores the practical applicability of these catalysts in large-scale ammonia production, addressing both efficiency and sustainability concerns.

The integration of advanced nanomaterials and surface modification techniques such as doping,[68-74] alloying,[75-79] and the creation of core-shell structures[80-87] continues to enhance the structural integrity and longevity of these catalysts through pathways such as doping, alloying, and core-shell structures. These methods not only improve catalytic activity but also mitigate common deactivation mechanisms such as leaching and fouling, ensuring sustained performance during prolonged operational cycles. Additionally, the scalability of synthesizing these heterostructured catalysts has been a focus, which is crucial for their implementation in industrial settings.

2.2. Single-Atom Catalysts (SAC)

SAC represent a sophisticated approach towards enhancing the precision of catalytic site design, which is crucial for achieving highly selective NO_3RR.[76,88-94] For instance, cobalt-copper mixed SACs utilize the distinct catalytic functions of cobalt and copper to optimize nitrate conversion. In this architecture, cobalt sites efficiently engage in reducing nitrate to nitrite, while copper sites undertake the subsequent reduction of nitrite to ammonia.[54,95,96] This sequence of reactions forms a tandem catalytic mechanism that has been shown to attain FE levels of up to 96%, along with significant ammonia production rates. Computational modeling has provided valuable insights into the electronic interactions between cobalt and copper, illustrating how the proximity of these metals enhances catalytic efficacy. This fine-tuning of active sites not only improves product selectivity but also ensures minimal side reactions, reinforcing the practicality of SACs in industrial applications. Further advancements in synthetic methods, such as atomic layer deposition, which allows precise control over the atomically dispersed sites,[97-99] and advanced nanostructuring techniques,[100-102] have opened avenues for developing SACs with unprecedented activity and selectivity for NO_3RR. The versatility of SACs is also highlighted by their ability to operate effectively under various reaction conditions, which can be tailored to maximize ammonia yields. This adaptability is beneficial for industrial settings, where fluctuating feedstock qualities and reaction parameters often necessitate flexible catalytic solutions. Moreover, studies indicate that SACs can be effectively integrated with other catalytic systems to create hybrid configurations that further enhance catalytic performance and efficiency in industrial applications.

2.3. Cascade Catalysis with Yolk-Shell Nanostructures

Recent progress in yolk-shell nanostructures has unveiled their considerable potential in achieving nearly complete conversion of nitrate to ammonia via cascade catalysis.[55,103-106] These innovative materials, such as the Cu_2O@CoO yolk-shell nanocubes, are designed to incorporate synergistic activity centers that facilitate stepwise NO_3RR (Figure 2g-k).[55] The layered architecture inherent in yolk-shell structures provides not only enhanced stability during catalytic reactions but also maintains robust performance over extended operational timelines. Remarkably, these catalysts have demonstrated FE exceeding 99%, in addition to achieving record-high ammonia yield rates within membrane electrolysis systems. The structural intricacies of yolk-shell nanostructures allow for the creation of spatially separated active sites, which can effectively target distinct reaction stages. This spatial design minimizes the diffusion barriers between intermediates, thus expediting the overall reaction kinetics. Moreover, the yolk-shell framework is conducive to maintaining a controlled environment for the catalytic process, protecting the active sites from deactivation while ensuring optimal interaction with reactants. Further refinements in yolk-shell nanostructure design,

 doi:10.20944/preprints202501.1574.v1

such as varying the shell thickness and optimizing the yolk composition, continue to strengthen their catalytic efficiency. Explorations into combining multi-metallic yolk-shell frameworks are particularly promising, as they could exploit cooperative effects between different catalytic metals, thereby enhancing selectivity even further. Recent developments also include the investigation of functionalizing yolk-shell structures with specific ligands or stabilizers that can enhance reaction mechanisms and improve product outcomes. The potential applications of these yolk-shell nanostructures are vast, extending beyond ammonia production to encompass other catalytic processes in environmental remediation and energy conversion technologies. Their resilience and efficiency position them as a significant advancement in the field of heterogeneous catalysis.

2.4. Summary of Innovations in Catalysis

Recent advances in catalytic materials, particularly through the development of heterostructured catalysts, SAC, and yolk-shell nanostructures, demonstrate transformative pathways for sustainable ammonia production. The integration of various materials in heterostructured catalysts has been pivotal in optimizing charge transfer and enhancing reaction kinetics, leading to impressive ammonia yield rates. Likewise, SACs offer a precision-driven approach to tailor catalytic mechanisms, which results in high selectivity and efficiency during NO_3RR processes. As innovations in catalyst design continue to progress, the utilization of novel nanostructures such as yolk-shell architecture exemplifies significant leaps in overall catalytic performance. With ongoing research and development efforts focused on optimizing these advanced catalysts, the landscape for sustainable ammonia synthesis will likely see further enhancements that not only improve efficiency but also address environmental challenges associated with traditional ammonia production methods. This exploration of cutting-edge catalytic technologies holds the promise of making sustainable ammonia synthesis a reality, consequently contributing to greener industrial practices for the next step which is the MEA level.

3. Membrane Electrode Assembly for Electrochemical Nitrate Reduction

3.1. MEA Configuration and Performance Indicators

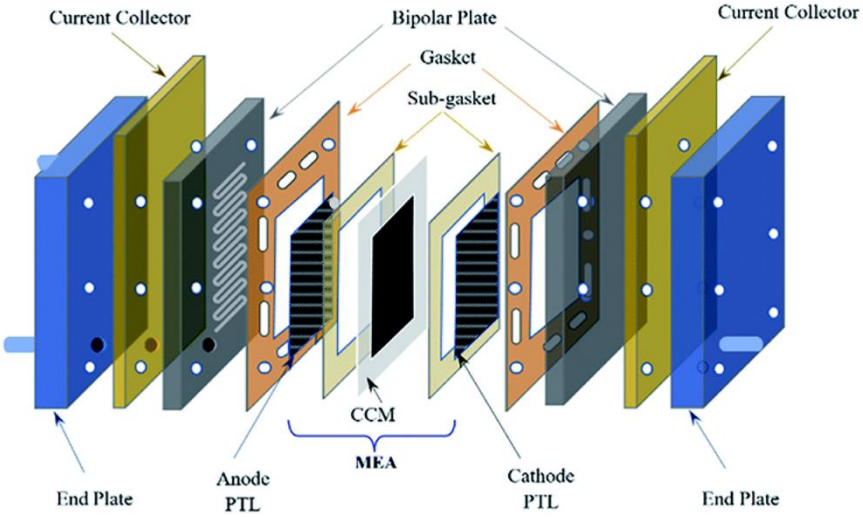

Figure 3. A schematic image of MEA configuration. Reproduced with permission from Ref. [107], Copyright (2022), The Royal Society of Chemistry.

Known as a zero-gap cell, the MEA configuration is essential for minimizing Ohmic resistance within the system. As shown in **Figure 3**, it consists of vital parts such as the anode plate, porous transport layer (PTL) on the anode side, catalytic layer (CL) for the anode, polymer electrolyte membrane (PEM), catalytic layer for the cathode, cathode PTL, and cathode plate. These components are combined into a cohesive unit through a hot-pressing process, forming the MEA's structural core. The PTL, which includes a support layer and a microporous layer, provides several beneficial

 doi:10.20944/preprints202501.1574.v1

properties. These include high levels of porosity, effective conduction of electricity, permeability to water, and robust mechanical strength, along with a carefully balanced hydrophobic and hydrophilic nature. PTLs not only transport reactants and products but also facilitate electron conduction while supporting the CL. The CL, where multiphase electrochemical reactions take place, is made of a catalyst combined with a binder. In NO_3RR research, a primary focus lies in creating electrocatalysts that deliver high activity, selectivity, stability, and cost-efficiency. Electrochemical nitrate reactions primarily occur at the solid-liquid interface (SLI) within the CL, where electrons, protons, and nitrate ions meet at the catalyst's active sites. To improve MEA performance, factors such as PTL properties, CL composition, and ionomer selection must be carefully optimized. PEMs serve as selective barriers between the anode and cathode, preventing the crossover of electrolytes and reaction products while maintaining ionic charge balance in the system. The ideal PEM should demonstrate superior ion conductivity (greater than 10^{-2} S cm^{-1}), excellent chemical and mechanical strength, and long-term stability under operational conditions.

To thoroughly evaluate the influence of electrolyzer design on the catalytic efficiency of NO_3RR, a variety of performance metrics have been employed. These include FE, current density, energy utilization efficiency, single-pass nitrate utilization efficiency (SPU), and system stability.

Faradaic Efficiency (FE): FE measures the proportion of the total charge utilized in forming the target product relative to the total charge passed through the system. It is an essential metric to assess the selectivity of the product and is defined as following equation.

$FE_i = Q_i/Q_{total} \times 100 = N_i \cdot n_i \cdot Q_{total} \times 100$, where FE_i: FE of product i (%), Q_i: Charge used for the formation of product i (C), Q_{total}: total consumed charge (C), Ni: amount of product i (mol), n_i: number of electrons transferred to generate product i, and F: Faraday constant (96485 C mol^{-1})

Current Density (*j*): current density, representing the electric current per unit area of the electrode, provides insights into the electrode's conductivity and the reaction rate of NO_3RR. It is influenced by factors like the catalyst's efficiency, the type and concentration of electrolyte, and the nitrate feed rate. It is calculated as

$j_{total} = i_{total}/S_{wE}$, $j_{partial,i} = j_{total} \cdot F \cdot E_i$, where i_{total}: total current (A), S_{wE}: working area of the electrode (cm^2).

Energy Efficiency (EE): this metric quantifies how effectively the energy is converted into the desired product. It evaluates the process's economic and industrial feasibility and is calculated as follows:

$EE_i = E°_{cell}/E_{cell} \cdot FE_i$, $E°_{cell} = \Delta G°/zF$, where $E°_{cell}$: Thermoneutral voltage, $\Delta G°$: Gibbs free energy change for the reaction (k*j*/mol), E_{cell}: Applied cell voltage (non-iR compensated), z: number of electrons transferred to form the product.

Single-pass Nitrate Utilization Efficiency (SPU): SPU reflects the efficiency of converting the input nitrate into products within a single pass through the electrolyzer. It is expressed as:

SPU = Converted nitrate/Input nitrate $\times$ 100

Stability: stability is a vital factor for evaluating the long-term reliability of the catalyst or reactor. It is assessed by monitoring the consistency of current density, product selectivity, and the physical or chemical properties of the catalyst during prolonged operation.

3.2. Role of Membranes in MEA Design

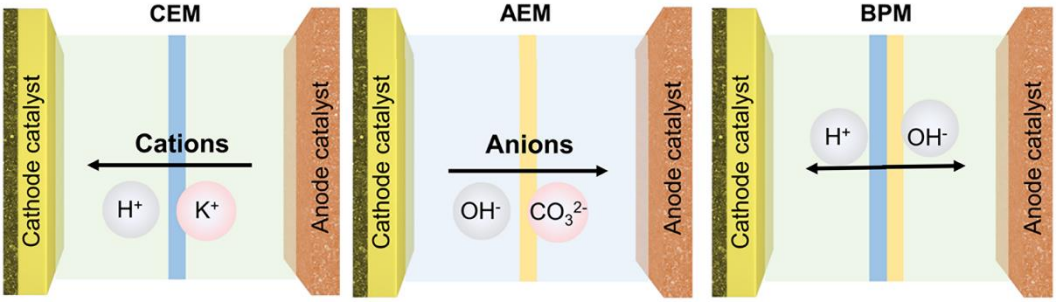

Figure 4. A schematic image of different types of membrane for MEA configuration. Reproduced with permission from Ref. [108], Copyright (2023), The Royal Society of Chemistry.

 doi:10.20944/preprints202501.1574.v1

Membranes are a critical component of MEA, serving as ion-conducting barriers that separate the anode and cathode compartments while facilitating selective ionic transport. The choice of membrane significantly impacts the electrochemical performance, stability, and overall efficiency of NO_3RR systems as shown in **Figure 4**.

Cation exchange membranes (CEM) are widely used in MEA systems due to their high proton conductivity and chemical stability especially in acidic environment. These membranes allow cations or protons (H^+) to transfer from the anode to the cathode while preventing crossover of reactants and products, ensuring system efficiency and selectivity. Nafion-117 was employed in several studies [109], [110], [111], to enable proton conduction in acidic or neutral environments. Nafion-117 acted as a solid electrolyte in a humidified environment, eliminating the need for liquid electrolytes. [109] This design achieved a FE of 92% for NO_3RR while suppressing hydrogen evolution reactions (HER). Additionally, its ability to prevent nitrate crossover maintained high ammonia selectivity. Nafion-117 membrane was coupled with CuZn alloy nanoparticles as the cathode, demonstrating superior performance with a FE of 97% and an ammonia yield of 3.6 $mmol \cdot h^{-1} \cdot cm^{-2}$.[110] The The robustness of Nafion-117 ensured consistent ionic transport even under high current densities. Nafion-115 was utilized in alongside Ag-doped Cu_2O nanocubes as the cathode. The thinner structure of Nafion-115, compared to Nafion-117, provided reduced ionic resistance, improving overall energy efficiency. This configuration achieved a FE of 93% and demonstrated the membrane's capability to balance proton conductivity and mechanical strength. [111]

Anion exchange membranes (AEM) facilitate the transport of hydroxide ions (OH^-) in alkaline environments, making them ideal for systems operating with alkaline electrolytes. Their stability in such conditions allows for efficient coupling with alkaline electrolytes and cathodic NO_3RR reactions (NO_3RR). FAA-3-50 membranes were employed to support NO_3RR under alkaline conditions. NiCo LDH on Cu nanowires was paired with FAA-3-50, achieving a FE of 94.25% at 570 mA cm^{-2}. The membrane's ability to provide consistent hydroxide ion transport while maintaining chemical stability was instrumental in achieving high efficiency and selectivity. [112]. Similarly, the FAA-3-50 membrane demonstrated compatibility with Co nanoparticles on 3D Cu foam, achieving an ammonia yield of 98.43 $mg \cdot h^{-1}$. [113] Its durability under high current densities highlighted its suitability for industrial applications. The PK-130 membrane was integrated into a glycerol oxidation coupled NO_3RR system [12]. This AEM supported Pd nanoparticles on Cu foam as the cathode and $NiCo_2O_4$ as the anode, achieving a FE of 97%. Its role in balancing ionic conductivity and mechanical stability under alkaline conditions was critical in maintaining long-term operational stability.

Bipolar membranes (BPM) combine the properties of proton exchange and anion exchange membranes, enabling the dissociation of water into H^+ and OH^- at their interfacial layer. This feature is particularly useful in driving NO_3RR reactions under dual pH conditions. BPM, such as Fumasep FBM, were employed to enhance the local reaction environment. Cu nanoparticles on carbon paper were paired with Fumasep BPMs, achieving a FE of 60.8%. [114] The BPM's ability to generate hydroxide ions locally improved NO_3RR kinetics, demonstrating its suitability for systems requiring dual-pH environments. Co–Cu single-atom/cluster catalysts were integrated with Fumasep FBM, achieving a FE of 91.2% over 32 hours. [88] The BPM's robust water dissociation capability contributed to stable and efficient operation, highlighting its potential for long-term NO_3RR applications.

Some studies employed specialized membranes to ensure durability and compatibility under harsh reaction conditions. X37-50 grade T (Dioxide Materials) membrane [115] demonstrated enhanced chemical stability in a NO_3RR system coupling ethylene glycol oxidation. This AEM maintained high FE (96.3 %) and durability under alkaline conditions, supporting extended operational periods at 100 mA cm^{-2}. Fumasep FAA-3 membrane was paired with Cu_3P-Ni_2P heterostructures, achieving a FE of >99%.[55] Its excellent ion transport properties and chemical resistance in alkaline media ensured efficient coupling between the cathode and anode reactions.

Membranes play a pivotal role in determining the performance, stability, and scalability of MEA-based NO_3RR systems. CEM enables efficient ionic transport and selectivity in acidic and neutral environments. AEM like FAA-3-50 and PK-130 exhibit excellent chemical stability and compatibility with alkaline conditions, while BPM such as Fumasep FBM provide unique dual-pH functionalities

 doi:10.20944/preprints202501.1574.v1

that enhance reaction kinetics. The choice of membrane must align with the system's operational parameters, including electrolyte composition, current density, and reaction stability. composition, current density, and reaction stability.

Table 1. Recently reported MEA electrolyzer for NO_3^-RR to NH_3.

Catholyte	Anolyte	Membrane type	Cathode material	Anode material	Counter oxidation reaction	Current Density	Voltage	NH_3 FE	NH_3 Yield	Ref.
1 M KOH with 0.1 M KNO_3	1 M KOH	CEM (Nafion 117)	Oxide-Derived Cu (OD-Cu) Mesh (40 mesh)	IrOx/Ti mesh	OER	400 mA cm^{-2}	n/a	90%	1.6 mmol h^{-1} cm^{-2}	[116]
1 M KOH with 2000 ppm NO_3^-	1 M KOH	AEM (FAA-3-50)	NiCo LDH on Cu nanowires (NiCo LDH/Cu NW)	Au-$Ni(OH)_2$	OER	~300 mA cm^{-2}	2 V	~90%	~1.6 mmol h^{-1} cm^{-2}	[112]
2000 ppm NO_3^- without supporting electrolyte	0.258 M NaOH	CEM (Nafion-117) with PSE layer	Ru-dispersed Cu nanowires (Ru-CuNW)	IrO_2	OER	100 mA cm^{-2}	~2.5 V	92%	Not explicitly stated	[109]
1 M KOH with 0.1 M KNO_3	1 M KOH	AEM (FAA-3-PK-130)	CoP-Cu/$Co(OH)_2$ heterojunction	S-(Ni,Fe)OOH	OER	275 mA cm^{-2} (60 ℃)	1.8 V	~90 % (60 ℃)	~1.4 mmol h^{-1} cm^{-2} (60 ℃)	[117]
1 M KOH with 0.1 M KNO_3	1 M KOH with 1 M ethylene glycol	AEM (X37-50 grade T)	Oxygen-deficient $NiCo_2O_4$ porous nanowires (Vo-$NiCo_2O_4$/NF)	Vo-$NiCo_2O_4$/NF	Ethylene Glycol Oxidation Reaction (EGOR)	100 mA cm^{-2}	1.53 V	96.3 %	0.36 mmol h^{-1} cm^{-2}	[115]
1 M KCl with 70 mM KNO_3	1 M KOH	BPM (Fumasep FBM)	Cu nanoparticles on carbon paper	Ni foam	OER	200 mA cm^{-2}	~5.5 V	60.8 %	Not explicitly stated	[114]

 doi:10.20944/preprints202501.1574.v1

0.5 M K_2CO_3										
0.5 M KOH with 0.1 M KNO_3	0.5 M KOH	AEM (Fumasep FAA-3)	Cu_2O@CoO yolk–shell nanocube	IrO_2	OER	~750 (375) mA cm^{-2}	1.9 V (2.3 V)	>99.85%	6.82 (31.50) mg h^{-1} cm^{-2}	[55]
1 M NaOH + 200 ppm of NO_3^-	1 M NaOH	AEM (Not specified)	Cu_3P-Ni_2P	Ir	OER	575 mA cm^{-2}	2.6 V	72%	1.9 mmol h^{-1} cm^{-2}	[110]
1 M KOH with 0.1 M KNO_3	1 M KOH	AEM (Fumasep FAA-3-50)	Co nanoparticles (CoNPs/CF)	Ni foam	OER	200 mA cm^{-2}	n/a	85.42 %	13.55 mg h^{-1} cm^{-2}	[113]
1 M KOH with 2 M KNO_3	1 M KOH	BPM (Fumasep FME)	Co–Cu mixed single-atom catalyst	Commercial Dimensionally Stable Anode (DSA) mesh	OER	100 mA cm^{-2}	From 3.5 to 4.5 V	From 85 to 65 %	1.03 M NH_3 after 32 h	[88]
1 M KOH with 0.1 M KNO_3	1 M KOH	CEM (Nafion 115)	Sputtered Cu	Ni foam	OER	395 mA cm^{-2}	3.5 V	91 %	30.26 mg h^{-1} cm^{-2}	[118]
1 M KOH with 0.1 M KNO_3	1 M KOH with 0.33 M glycerol	AEM (PK-130, JBOKE New Materials Technology Co., LTD.)	Pd nanoparticles on Cu foam	$NiCo_2O_4$	Glycerol Oxidation Reaction (GOR)	~150 mA cm^{-2}	1.6 V	96 %	~20 mg h^{-1} cm^{-2}	[111]

3.3. Optimization Through Operating Variations

In a MEA configuration, the operating variations are pivotal to influence the ammonia conversion efficiency and product selectivity. The sequential nitrate-to-ammonia reduction reaction ($NO_3^- \rightarrow NO_2^- \rightarrow NH_3$) involves a mainly two-step pathway where the residence time of intermediates and the availability of electrons are crucial. Therefore, these parameters can be controlled by adjusting proton availability, the catholyte flow rate and current density, enabling the optimization of reaction conditions for ammonia production.

 doi:10.20944/preprints202501.1574.v1

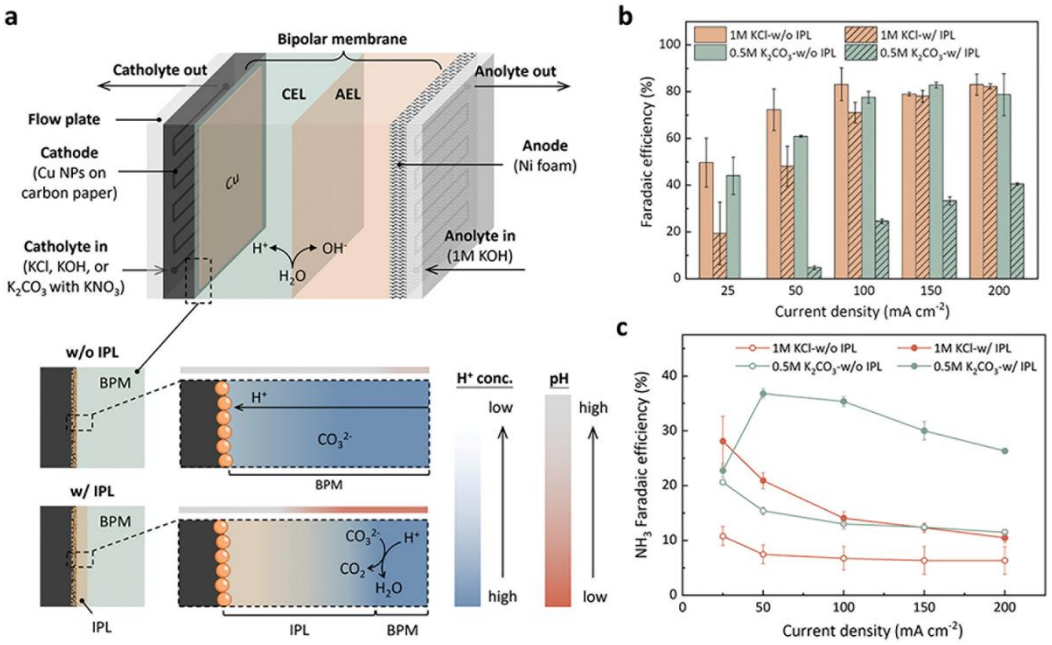

Figure 5. **(a)** A schematic representation of a BPM-based MEA electrolyzer, illustrating the pH gradient within the interfacial polymer layer (IPL) and its effect on proton inhibition in the BPM-MEA system. **(b)** FE of the hydrogen evolution reaction (HER) in 1 M KCl and 0.5 M K_2CO_3 electrolytes containing 70 × 10^{-3} M KNO_3, measured across applied current densities ranging from 25 to 200 mA cm^{-2}. Diagonally striped bars represent electrolysis conducted with an interposer layer (IPL) present. **(c)** NH_3 FE in 1 M KCl and 0.5 M K_2CO_3 electrolytes containing 70 × 10^{-3} M KNO_3, with and without the interposer layer (IPL), measured across applied current densities ranging from 25 to 200 mA cm^{-2}. Reproduced with permission from Ref. [114], Copyright (2024), John Wiley & Sons.

In a BPM-MEA system, the regulation of proton flux is critical for optimizing NH_3 production. P.-W. Huang et al. demonstrated that incorporating an interposer layer (IPL) between the BPM and the catalyst effectively inhibited proton transfer, reducing the competitive HER at higher current densities (**Figure 5a**). [114] For instance, with the combination of a 0.5 M K_2CO_3 electrolyte and an IPL, HER FE was reduced to 40 % at 200 mA cm^{-2}, compared to 80 % without these modifications (**Figure 5b**). This adjustment enhanced NH_3 production, achieving a peak FE of 60.8 % (**Figure 5c**). Furthermore, the reverse electrode configuration (where the catalyst faces away from the BPM) minimized diffusion resistance for NO_3^- while increasing the transport path for protons and CO_2. This design further reduced HER and improved NH_3 production efficiency by leveraging the directional transport dynamics within the BPM-MEA system.

Similarly, T. Yuan et al. investigated the sequential reduction of nitrate (NO_3^-) to nitrite (NO_2^-) and finally to NH_3, emphasizing the role of proton flux. [118] They utilized a high flow catholyte (20 mL min^{-1}) to suppress HER and favor NH_3 selectivity at elevated current densities (up to 395 mA cm^{-2}). This setup achieved 91 % NH_3 FE, highlighting the necessity of balancing proton supply and reactant residence times to optimize product selectivity. Moreover, control over the residence time of intermediates, particularly NO_2^-, is a decisive factor in MEA performance. Low catholyte flow rates (1 mL min^{-1}) favored NH_3 production (61.3 % FE) but also led to higher HER due to prolonged intermediate interaction with protons. Conversely, higher flow rates (20 mL min^{-1}) mitigated HER but resulted in unconverted NO_2^- escaping the system. The optimized flow rate of 10 mL min^{-1} balanced NH_3 selectivity and minimized NO_2^- accumulation, achieving a peak partial current density for NH_3 of ~125 mA cm^{-2}. Current density also plays a pivotal role in determining product selectivity and reaction efficiency in MEA systems. Higher current densities (up to 395 mA cm^{-2}) significantly improved NH_3 FE, reaching a peak of 91 %, while suppressing competing reactions such as HER. However, at lower current densities (<100 mA cm^{-2}), the insufficient proton supply resulted in increased NO_2^- production due to incomplete reduction. This demonstrates the importance of maintaining a balance between electron supply and intermediate availability.

 doi:10.20944/preprints202501.1574.v1

3.4. Coupling Counter Reactions

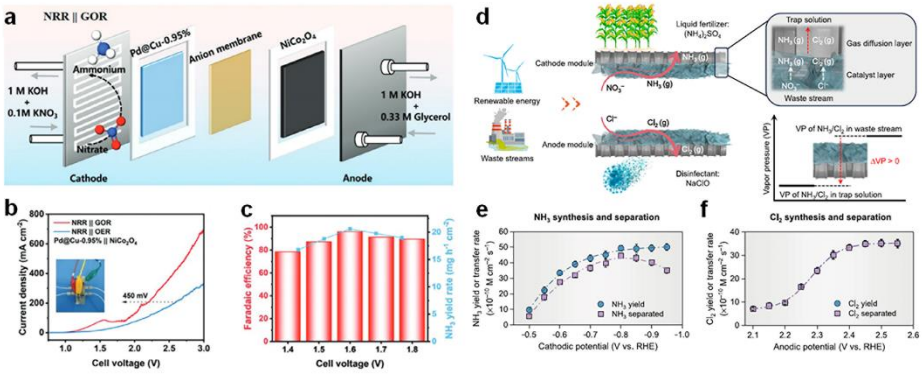

Figure 6. (a) A schematic illustration depicts a paired electrochemical refinery, utilizing a Pd@Cu-0.95% cathode for NO_3RR and a $NiCo_2O_4$ anode for glycerol oxidation (GOR), enabling the simultaneous production of high-value products, ammonium, and formate. **(b)** Linear sweep voltammetry (LSV) curves compare the paired electrochemical refinery's performance with and without glycerol at the anode. The inset shows a digital photograph of the actual paired electrochemical refinery setup, featuring the Pd@Cu-0.95% cathode and $NiCo_2O_4$ anode, designed to co-upgrade nitrate and glycerol into ammonium and formate. **(c)** The relationship between ammonium yield and FE is presented as a function of cell voltage in a custom-designed flow refinery. Reproduced with permission from Ref. [111], Copyright (2024), John Wiley & Sons. (d) A schematic of the electrochemical NH_3 and Cl_2 production under ambient conditions using renewable energy and waste stream. (e, f) The yield and separation rates of NH_3 and Cl_2 as a function of applied potentials on cathodic and anodic electrode assemblies, respectively. Reproduced with permission from Ref. [38], Copyright (2024), Springer Nature.

The efficiency and overall feasibility of the electrochemical NO_3RR reaction (NO_3RR) heavily depend on the oxidation reaction occurring at the anode. These counter reactions not only balance the electron flow in the system but also influence the energy efficiency and stability of the process. The coupling of complementary oxidation reactions has been explored extensively, leading to significant advancements in system performance. The oxygen evolution reaction (OER) emerged as the primary anodic process. For example, in systems using IrO_2 as the anode material, OER served as a stable and efficient counter-reaction, demonstrated that coupling NO_3RR with Cu mesh at the cathode with OER at the anode yielded a FE of 90 % for NO_3RR, highlighting the compatibility of this reaction in alkaline electrolytes. [116] Similarly, the combination of a CoP-Cu/$Co(OH)_2$ cathode with an S-(Ni,Fe)OOH anode for OER resulted in a record-high ammonia yield of 9.91 mmol h^{-1} cm^{-2}, further showcasing the synergy between these reactions. [117] While most studies utilized traditional oxidation reactions, some explored innovative approaches to enhance anodic performance. J. Suh et al. employed a dimensionally stable anode (DSA) mesh to support OER in a system using Co–Cu single-atom/cluster catalysts at the cathode. The stable operation of the DSA ensured efficient NO_3RR with a FE of 91.2 % over 32 hours of continuous operation. [88]

In some cases, the choice of counter-reaction was strategically altered to improve the energy efficiency of the system. For instance, ethylene glycol oxidation (EGOR) was employed as the anodic reaction, leveraging its lower overpotential compared to OER with the co-production of valuable formate with a high FE (94.89 % at 1.35 V vs RHE). The oxygen-deficient $NiCo_2O_4$ nanowires used as the anode in this study achieved a NH_3 FE of 96.3 % at 100 mA cm^{-2} by applying 1.53 V , demonstrating the potential of alternative anodic reactions to enhance overall system efficiency. [115] The integration of glycerol oxidation (GOR) as a counter-reaction was explored [111], where Pd nanoparticles on Cu foam were used as the cathode and $NiCo_2O_4$ as the anode (**Figure 6a**). The incorporation of glycerol into the electrolyte resulted in a significant reduction in cell voltage, with a 450 mV drop observed at a current density of 200 mA cm^{-2} (**Figure 6b**). This system achieved a FE of 96 % at a cell voltage of 1.6 V, demonstrating high selectivity and efficiency for simultaneous ammonium and formate production (**Figure 6c**). The stability tests of the system confirmed excellent operational durability over a 10-hour period at 200 mA cm^{-2}, highlighting the feasibility of integrating

 doi:10.20944/preprints202501.1574.v1

glycerol oxidation with NO_3RR for sustainable chemical synthesis. The chlorine evolution reaction (CER) was also coupled with NO_3RR in a membrane-free configuration (**Figure 6d**). [38] Using RuO_2 as the anode, this system simultaneously produced ammonia and chlorine gas, targeting the production of chlorine gas (Cl_2) from chloride ions (Cl^-). Using a synthetic medium containing 25 mM NO_3^- and Cl^-, At a cathodic potential of −0.80 V versus RHE, a peak NH_3 yield rate of approximately 49.4 × 10^{-10} M-NH_3 $cm^{-2}{\cdot}s^{-1}$ was achieved, alongside a high separation efficiency of 90 % (**Figure 6e)**. At this potential of the anodic potential applied ranged up to 2.45 V vs RHE, a maximum Cl_2 yield rate of approximately 35.2 × 10^{-10} M-Cl_2 $cm^{-2}{\cdot}s^{-1}$ was achieved, reflecting efficient catalytic performance (**Figure 6f**). The setup was further optimized in a co-electrosynthesis system where NO_3RR occurred at the cathode and chlorine evolution at the anode. With a total cell potential of 3.0 V, the recovery efficiency of Cl_2 improved to 96 %, while product loss was minimized to 5 %. Simultaneously, ammonia production at the cathode achieved a high recovery efficiency of 90-96 %, with minimal nitrogen loss as N_2. Overall, the choice of anodic reaction significantly influences the system's performance metrics, such as energy efficiency, ammonia yield, and operational stability. The coupling of NO_3RR with OER remains a widely adopted strategy due to its simplicity and robustness. However, the exploration of alternative anodic reactions offers promising avenues for improving system efficiency and co-product valorization. Future research should focus on optimizing these counter-reactions and exploring new anodic processes to further enhance the practicality of electrochemical NO_3RR systems.

3.5. Functionalized Electrolyzer Configurations

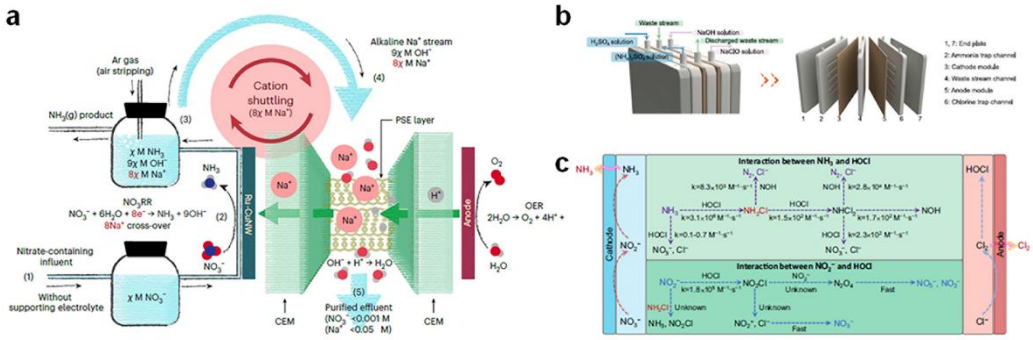

Figure 7. (a) A schematic outlines the proposed process for nitrate (NO_3^-) influent treatment using a PSE reactor without supporting electrolytes. NO_3^- influent (χ = 0.0323 M unless specified) is introduced into the reactor, where electrochemical NO_3RR converts NO_3^- to ammonia (NH_3). Cations migrate from the PSE layer to the cathode through the membrane, providing a cation shielding effect. Following catalysis, NH_3 is purified via air stripping, while the remaining stream, containing crossover cations, is recirculated to the PSE layer in a closed loop, ensuring no net cation consumption. The treated effluent passes through the PSE layer, achieving NO_3^- and Na^+ concentrations of <0.001 M and <0.05 M, respectively, under conditions assuming complete NO_3^- conversion and Na^+ crossover. Reproduced with permission from Ref. [109], Copyright (2024), Springer Nature. **(b)** ASchematics and configuration of this flow-type membrane-free electrolyzer for electrochemical synthesis and in situ recovery of ammonium sulfate and hypochlorous acid from waste streams. **(c)** The major heterogeneous and homogeneous redox reactions within the electrolyzer. Reproduced with permission from Ref. [38], Copyright (2024), Springer Nature.

F. -Y. Chem et al. introduces a porous solid-state electrolyte (PSE) reactor that facilitates efficient electrochemical NO_3RR to ammonia while eliminating the need for high-concentration supporting electrolytes (**Figure 7a**). A key idea lies in the use of a styrene–divinylbenzene sulfonated co-polymer as the middle PSE layer, enabling a cation shielding mechanism. This layer plays a pivotal role in regulating ion transport and mitigating parasitic HER at the cathode. Sodium ions (Na^+) are shuttled across the middle PSE layer from the anode to the cathode. This ion transport is driven by the concentration gradient and serves to maintain electroneutrality during the reaction. Importantly, this cation shuttling process enhances the local concentration of Na^+ at the cathode–membrane interface, displacing protons (H^+) and thereby suppressing HER. This suppression ensures that a higher

 doi:10.20944/preprints202501.1574.v1

proportion of the electrons are directed toward NO_3RR rather than side reactions. Under operational conditions with a 2000 ppm nitrate influent, the PSE reactor achieves an exceptional NH_3 FE of 92 % at a current density of 100 mA cm^{-2}. The PSE reactor also demonstrates impressive long-term stability, retaining over 90 % of its NH3 FE across ten operational cycles (10 days). This stability is attributed to the robust cation exchange process within the middle chamber, which prevents cross-migration of nitrate ions to the anode and ensures sustained suppression of HER. Furthermore, air stripping of the catholyte efficiently separates NH_3 gas, achieving a stripping efficiency exceeding 95 %. [109] J. Gao et al. also presents a flow-type, membrane-free electrolyzer that synchronously produces and separates ammonia (NH_3) and chlorine gas (Cl_2) from waste streams containing nitrate (NO_3^-) and chloride (Cl^-) (**Figure 7b**). By integrating gas-extraction electrodes, the system eliminates the need for ion-selective membranes while maintaining high product purity and minimizing product loss. The system consists of three chambers: cathodic, anodic, and a central waste stream channel. Especially, the middle waste stream channel serves as the source of NO_3^- and Cl^-, which diffuse toward their respective electrodes. Gas-extraction electrodes are used to transfer NH_3 and Cl_2 across the gas diffusion layers into separate trap solutions. In the ammonia trap channel, circulating H_2SO_4 (pH 1.0 ± 0.1) reacts with NH_3 to form ammonium sulfate $(NH_4)_2SO_4$). Similarly, in the chlorine trap channel, circulating NaOH (pH 13.0 ± 0.1) converts Cl_2 to sodium hypochlorite (NaClO) (**Figure 7c**). The electrolyzer achieves high product recovery efficiencies, with NH_3 and Cl_2 separation efficiencies reaching 90% and 99%, respectively, at a cell potential of 3.0 V. The total energy consumption for simultaneous production of $(NH_4)_2SO_4$ and NaClO is calculated to be 7.1 kWh per kilogram of combined products. After 6 hours of operation with a reverse osmosis retentate waste stream, the system produced $(NH_4)_2SO_4$ at a concentration of 83.8 mM and NaClO at 243.4 mM. The gas-extraction process effectively prevents the interaction between NH_3 and Cl_2, which could otherwise result in undesired by-products such as nitrogen gas (N_2) and chloride ions (Cl^-). This design minimizes residual nitrogen- and chlorine-containing species in the waste stream, ensuring compliance with discharge regulations. Specifically, residual NH_3/NH_4^+, Cl_2/HClO/ClO^-, and NO_2^- concentrations were measured at 0.32 mM, 0.06 mM, and 0.15 mM, respectively. [38]

5. Discussion and Future Directions

5.1. Advancements in Electrolyzer Designs

MEAs represent a significant advancement in electrolyzer technology, achieving 99.8% nitrate-to-ammonia conversion in industrial wastewater applications. These systems enhance operational stability by integrating efficient proton transport mechanisms, minimizing side reactions like hydrogen evolution. Similarly, membrane-free electrolyzers simplify system architecture and reduce costs, achieving FE exceeding 90% and ammonia yield rates of over 3.6 $mmol \cdot h^{-1} \cdot cm^{-2}$ under optimized conditions. These designs reduce internal resistance, enhance energy efficiency, and are well-suited for large-scale applications.

5.2. Catalyst Innovations Catalyst Innovation

Catalyst innovation has driven improvements in NO_3RR performance, with heterostructured catalysts, SAC, and yolk-shell nanostructures achieving outstanding metrics.

- **Heterostructured Catalysts:** Cu-Ni phosphide catalysts have demonstrated FE exceeding 90% and ammonia yield rates surpassing 1.9 $mmol \cdot h^{-1} \cdot cm^{-2}$ in PEMEA systems.
- **Single-Atom Catalysts (SACs):** Tandem catalytic mechanisms of SACs have achieved FE as high as 96%, optimizing nitrate-to-ammonia conversion by leveraging site-specific activity.
- **Yolk-Shell Nanostructures:** Cu_2O@CoO yolk-shell nanocubes have exhibited over 99% FE, coupled with record-high ammonia yield rates in MEA systems.

Recent breakthroughs include 3D copper foam-supported cobalt nanoparticles (CoNPs/CF), which achieved a FE of 92% and ammonia yield rates of 14.3 $mg \cdot h^{-1} \cdot cm^{-2}$. Furthermore, CoP-Cu/$Co(OH)_2$ systems have delivered 9.91 $mmol \cdot h^{-1} \cdot cm^{-2}$ ammonia generation with FE exceeding 99.2% under industrial-level current densities.

5.3. Integration with Wastewater Treatment

 doi:10.20944/preprints202501.1574.v1

The integration of NO_3RR with wastewater treatment processes provides a dual advantage: mitigating nitrate pollution while generating valuable products such as ammonia, ammonium sulfate, and sodium hypochlorite. Membrane-free electrolyzers and advanced modules have demonstrated robust performance in treating the industrial brine, achieving compliance with stringent discharge regulations. This approach offers a cost-effective pathway for ammonia production and waste stream valorization, highlighting its potential for large-scale implementation.

Recent advances in coupling NO_3RR with ethylene glycol oxidation reactions (EGOR) exemplify an innovative, energy-saving electrosynthesis strategy. Oxygen-deficient $NiCo_2O_4$ porous nanowire arrays, optimized for oxygen vacancies and featuring a unique nanowire structure, have achieved over 96.3% FE for ammonia and 94.2% for formate production at low operating voltages in MEA systems. These catalysts demonstrate excellent stability over 120 hours, reinforcing their scalability and suitability for sustainable ammonia production. The integration of EGOR with NO_3RR reduces energy consumption significantly compared to conventional OER-based systems, showcasing the synergistic advantages of co-production strategies.

5.4. Optimizing Reaction Conditions

Optimizing reaction conditions, such as catholyte flow rates, current densities, and residence times, is essential for maximizing NO_3RR performance. Tailored MEA configurations and sequential reduction systems have proven effective in significantly improving ammonia selectivity and FE. For instance, coupling NO_3RR with ethylene glycol oxidation (EGOR) has reduced energy consumption and facilitated the co-production of valuable chemicals, underscoring the role of advanced engineering principles in driving these advancements.

Recent studies highlight the importance of precise adjustments to catholyte flow rates and current densities in enhancing the interaction between nitrate and nitrite intermediates, ensuring high selectivity for ammonia production. Advanced MEA setups control reactant residence times, minimizing undesired HER while enhancing nitrite-to-ammonia conversion. Single-pass operations exemplify the scalability of these approaches, achieving up to 91% FE for ammonia synthesis under industrially relevant current densities. These findings pave the way for high-performance NO_3RR systems suitable for both wastewater remediation and decentralized ammonia production, reinforcing their potential for large-scale implementation.

5.5. Future Directions

While significant progress has been made, challenges such as catalyst durability, competitive hydrogen evolution, and scalability remain critical barriers to widespread implementation. Future research should focus on developing durable, cost-effective catalysts and optimizing reactor designs for energy efficiency. Additionally, integrating NO_3RR with renewable energy systems and complementary processes will be crucial for enabling its adoption on a broader scale.

Translating laboratory successes to pilot and industrial levels remains a key priority, as this step is essential for realizing the practical potential of NO_3RR technologies. The advancements reviewed highlight the transformative potential of NO_3RR as a cornerstone technology for sustainable ammonia synthesis and nitrate remediation. NO_3RR can significantly contribute to global sustainability goals. The focus should be on creating holistic systems that integrate environmental and industrial solutions, ensuring the long-term impact and scalability of these technologies.

6. Conclusions

Electrocatalytic NO_3RR to ammonia is a transformative solution for sustainable nitrogen management, addressing both ammonia production and nitrate pollution. Recent advancements in catalyst design, such as heterostructured catalysts, SAC, and yolk-shell nanostructures, have significantly enhanced NO_3RR efficiency and selectivity. These catalysts optimize reaction pathways and reduce energy requirements while achieving high FE and stability.

Innovations in electrolyzer designs, including PEMEA and membrane-free reactors, have improved scalability and energy efficiency, enabling near-complete nitrate-to-ammonia conversion

 doi:10.20944/preprints202501.1574.v1

in industrial conditions. Mechanistic studies have further bridged experimental and theoretical understanding, guiding the design of next-generation catalysts and reactors.

Despite progress, challenges such as hydrogen evolution, catalyst durability, and scalability persist, requiring interdisciplinary collaboration to overcome. Future research should focus on cost-effective catalysts, energy-efficient designs, and integration with wastewater treatment and renewable energy systems. NO_3RR electrolyzer offers significant promise as a sustainable alternative to traditional ammonia synthesis methods, with the potential to revolutionize ammonia production and nitrate remediation, contributing to global sustainability goals and a greener future.

Author Contributions: Conceptualization, K.H.K., and J.L.; writing-original draft preparation, K.H.K., and J.L; writing-review and editing, K.H.K., and J.L; supervision, J.L.; project administration, K.H.K., and J.L; funding acquisition, K.H.K. All authors have read and agreed to the published version of the manuscript.

Funding: This work was supported by the National Research Foundation of Korea (NRF) grant funded by the Korea government (MSIT) (RS-2024-003954830).

Data Availability Statement: Date are contained within the article.

Conflicts of Interest: The authors declare no conflicts of interest.

References

1. Liu, Y.-H.; Vu, M.H.; Lim, J.; Do, T.-O.; Hatzell, M.C. Influence of carbonaceous species on aqueous photo-catalytic nitrogen fixation by titania. *Faraday Discussions* **2019**, *215*, 379-392.
2. Fernandez, C.A.; Hortance, N.M.; Liu, Y.-H.; Lim, J.; Hatzell, K.B.; Hatzell, M.C. Opportunities for intermediate temperature renewable ammonia electrosynthesis. *Journal of Materials Chemistry A* **2020**, *8*, 15591-15606.
3. Hasan, M.H.; Mahlia, T.M.I.; Mofijur, M.; Rizwanul Fattah, I.; Handayani, F.; Ong, H.C.; Silitonga, A. A comprehensive review on the recent development of ammonia as a renewable energy carrier. *Energies* **2021**, *14*, 3732.
4. de la Hera, G.; Ruiz-Gutiérrez, G.; Viguri, J.R.; Galán, B. Flexible Green Ammonia Production Plants: Small-Scale Simulations Based on Energy Aspects. *Environments* **2024**, *11*, 71.
5. Chong, K.S.; Hamid, M.A.; Ng, D.K. Systematic decision-making framework for evaluation of process alternatives for sustainable ammonia (NH3) production. *Materials Today: Proceedings* **2022**, *64*, A6-A17.
6. Akay, G. Hydrogen, Ammonia and Symbiotic/Smart Fertilizer Production Using Renewable Feedstock and CO2 Utilization through Catalytic Processes and Nonthermal Plasma with Novel Catalysts and In Situ Reactive Separation: A Roadmap for Sustainable and Innovation-Based Technology. *Catalysts* **2023**, *13*, 1287.
7. Ye, M.; Jiang, X.; Zhang, Y.; Liu, Y.; Liu, Y.; Zhao, L. Enhanced Electrocatalytic Nitrate Reduction to Ammonia Using Functionalized Multi-Walled Carbon Nanotube-Supported Cobalt Catalyst. *Nanomaterials* **2024**, *14*, 102.
8. Khan, M.N.; Mohammad, F. Eutrophication: challenges and solutions. *Eutrophication: Causes, Consequences and Control: Volume 2* **2014**, 1-15.
9. Moloantoa, K.M.; Khetsha, Z.P.; Van Heerden, E.; Castillo, J.C.; Cason, E.D. Nitrate water contamination from industrial activities and complete denitrification as a remediation option. *Water* **2022**, *14*, 799.
10. Lazar, L.; Boicenco, L.; Pantea, E.; Timofte, F.; Vlas, O.; Bișinicu, E. Modeling Dynamic Processes in the Black Sea Pelagic Habitat—Causal Connections between Abiotic and Biotic Factors in Two Climate Change Scenarios. *Sustainability* **2024**, *16*, 1849.
11. Anaya-Rodríguez, F.; Durán-Álvarez, J.C.; Drisya, K.; Zanella, R. The challenges of integrating the principles of green chemistry and green engineering to heterogeneous photocatalysis to treat water and produce green H2. *Catalysts* **2023**, *13*, 154.
12. Fan, J.; Yang, L.; Ye, L.; Mei, M.; Zhu, W. Electrode Materials for NO Electroreduction Based on Dithiolene Metal–Organic Frameworks: A Theoretical Study. *Catalysts* **2024**, *14*, 739.
13. Yu, J.; Du, Y.; Liu, S.; Liu, Y.; Li, Y.; Cheng, Y.; Cao, P.; Zhang, X.; Yuan, X.; Liu, N. Co-Carbonization of Straw and ZIF-67 to the Co/Biomass Carbon for Electrocatalytic Nitrate Reduction. *Catalysts* **2024**, *14*, 817.

14. Zeng, K.-Y.; Wang, J.-J.; Fang, X.; Li, Z.-X. One Bicopper Complex with Good Affinity to Nitrate for Highly Selective Electrocatalytic Nitrate Reduction to Ammonia. *Catalysts* **2022**, *12*, 1561.
15. Kim, K.-H.; Lee, H.; Huang, X.; Choi, J.H.; Chen, C.; Kang, J.K.; O'Hare, D. Energy-efficient electrochemical ammonia production from dilute nitrate solution. *Energy & Environmental Science* **2023**, *16*, 663-672, doi:10.1039/D2EE03461A.
16. Guo, F.; Chen, Q.; Liu, Z.; Cheng, D.; Han, N.; Chen, Z. Repurposing mining and metallurgical waste as electroactive materials for advanced energy applications: advances and perspectives. *Catalysts* **2023**, *13*, 1241.
17. Lim, J.; Liu, C.-Y.; Park, J.; Liu, Y.-H.; Senftle, T.P.; Lee, S.W.; Hatzell, M.C. Structure sensitivity of Pd facets for enhanced electrochemical nitrate reduction to ammonia. *ACS Catalysis* **2021**, *11*, 7568-7577.
18. Lim, J.; Fernández, C.A.; Lee, S.W.; Hatzell, M.C. Ammonia and Nitric Acid Demands for Fertilizer Use in 2050. *ACS Energy Letters* **2021**, *6*, 3676-3685.
19. Chen, T.; Li, Y.; Li, L.; Zhao, Y.; Shi, S.; Jiang, R.; Ma, H. Cu modified Pt nanoflowers with preferential (100) surfaces for selective electroreduction of nitrate. *Catalysts* **2019**, *9*, 536.
20. Lee, H.; Kim, K.H.; Rao, R.R.; Park, D.G.; Choi, W.H.; Choi, J.H.; Kim, D.W.; Jung, D.H.; Stephens, I.E.L.; Durrant, J.R.; et al. A hydrogen radical pathway for efficacious electrochemical nitrate reduction to ammonia over an Fe-polyoxometalate/Cu electrocatalyst. *Mater Horiz* **2024**, *11*, 4115-4122, doi:10.1039/d4mh00418c.
21. Yang, Y.; Wang, H.; Wang, C.; Liu, J.; Wu, H.; Liu, N.; Wang, Q.; Shang, Y.; Zheng, J. Novel 2D Material of MBenes: Structures, Synthesis, Properties, and Applications in Energy Conversion and Storage. *Small* **2024**, *20*, 2405870.
22. Zhang, S.; Zhang, R.; Guo, Y.; Zhi, C. Ammonia Synthesis from Nitrate Reduction by the Modulation of Built-in Electric Field and External Stimuli. *EES Catalysis* **2025**.
23. Liu, K.; Li, H.; Xie, M.; Wang, P.; Jin, Z.; Liu, Y.; Zhou, M.; Li, P.; Yu, G. Thermally Enhanced Relay Electrocatalysis of Nitrate-to-Ammonia Reduction over Single-Atom-Alloy Oxides. *Journal of the American Chemical Society* **2024**, *146*, 7779-7790.
24. Yin, S.; Cao, R.; Han, Y.; Shang, J.; Zhang, J.; Jiang, W.; Liu, G. Electrocatalysts with atomic-level site for nitrate reduction to ammonia. *Journal of Energy Chemistry* **2024**.
25. Huang, T.; Liang, T.; You, J.; Huo, Q.; Qi, S.; Zhao, J.; Meng, N.; Liao, J.; Shang, C.; Yang, H. Coordination environment-tailored electronic structure of single atomic copper sites for efficient electrochemical nitrate reduction toward ammonia. *Energy & Environmental Science* **2024**, *17*, 8360-8367.
26. Yu, X.; Deng, J.; Liu, Y.; Jing, L.; Hou, Z.; Pei, W.; Dai, H. Single-atom catalysts: Preparation and applications in environmental catalysis. *Catalysts* **2022**, *12*, 1239.
27. Shen, S.; Sun, Y.; Sun, H.; Pang, Y.; Xia, S.; Chen, T.; Zheng, S.; Yuan, T. Research progress in ZIF-8 derived single atomic catalysts for oxygen reduction reaction. *Catalysts* **2022**, *12*, 525.
28. Li, S.; Ma, P.; Yang, J.; Krishnan, S.; Kesavan, K.S.; Xing, R.; Liu, S. Facile construction of three-dimensional heterostructured CuCo2S4 bifunctional catalyst for alkaline water electrolysis. *Catalysts* **2023**, *13*, 881.
29. Sanchis, I.; Rodriguez, J.J.; Mohedano, A.F.; Diaz, E. Activity and stability of Pd bimetallic catalysts for catalytic nitrate reduction. *Catalysts* **2022**, *12*, 729.
30. Shaheen, S.; Sadiq, I.; Ali, S.A.; Ahmad, T. Bismuth-based multi-component heterostructured nanocatalysts for hydrogen generation. *Catalysts* **2023**, *13*, 295.
31. Ye, W.; Zhang, Y.; Chen, L.; Wu, F.; Yao, Y.; Wang, W.; Zhu, G.; Jia, G.; Bai, Z.; Dou, S. A strongly coupled metal/hydroxide heterostructure cascades carbon dioxide and nitrate reduction reactions toward efficient urea electrosynthesis. *Angewandte Chemie International Edition* **2024**, *63*, e202410105.
32. Júnior, A.A.d.T.; Ladeira, Y.F.X.; França, A.d.S.; Souza, R.O.M.A.d.; Moraes, A.H.; Wojcieszak, R.; Itabaiana Jr, I.; Miranda, A.S.d. Multicatalytic hybrid materials for biocatalytic and chemoenzymatic cascades—Strategies for multicatalyst (Enzyme) co-immobilization. *Catalysts* **2021**, *11*, 936.
33. Pérez-Mayoral, E.; Godino-Ojer, M.; Matos, I.; Bernardo, M. Opportunities from Metal Organic Frameworks to Develop Porous Carbons Catalysts Involved in Fine Chemical Synthesis. *Catalysts* **2023**, *13*, 541.

34. Kim, J.; Han, G.H.; Seo, J.Y.; Kang, M.; Seo, M.-g.; Choi, Y.; Kim, S.Y.; Ahn, S.H. Improved CO Selectivity via Anion Exchange Membrane Electrode Assembly-Type CO2 Electrolysis with an Ionomer-Coated Zn-Based Cathode. *International Journal of Energy Research* **2024**, *2024*, 8984734.
35. Pushkarev, A.S.; Pushkareva, I.V.; du Preez, S.P.; Bessarabov, D.G. PGM-free electrocatalytic layer characterization by electrochemical impedance spectroscopy of an anion exchange membrane water electrolyzer with Nafion ionomer as the bonding agent. *Catalysts* **2023**, *13*, 554.
36. Kang, Y.; Kim, T.; Jung, K.Y.; Park, K.T. Recent progress in electrocatalytic CO2 reduction to pure formic acid using a solid-state electrolyte device. *Catalysts* **2023**, *13*, 955.
37. Zhang, G.; Li, B.; Shi, Y.; Zhou, Q.; Fu, W.-J.; Zhou, G.; Ma, J.; Yin, S.; Yuan, W.; Miao, S. Ammonia recovery from nitrate-rich wastewater using a membrane-free electrochemical system. *Nature Sustainability* **2024**, *7*, 1251-1263.
38. Gao, J.; Ma, Q.; Wang, Z.; Rittmann, B.E.; Zhang, W. Direct electrosynthesis and separation of ammonia and chlorine from waste streams via a stacked membrane-free electrolyzer. *Nat Commun* **2024**, *15*, 8455, doi:10.1038/s41467-024-52830-4.
39. Rajalekshmi, S.; Kumar, S.M.S.; Pandikumar, A. Exploring transition metal hydroxides performance in membrane-free electrolyzer based decoupled water splitting for step-wise production of hydrogen and oxygen. *Chemical Engineering Journal* **2024**, *496*, 154215.
40. Liu, D.; Qiao, L.; Peng, S.; Bai, H.; Liu, C.; Ip, W.F.; Lo, K.H.; Liu, H.; Ng, K.W.; Wang, S. Recent advances in electrocatalysts for efficient nitrate reduction to ammonia. *Advanced Functional Materials* **2023**, *33*, 2303480.
41. Fan, X.; Franch, C.; Palomares, E.; Lapkin, A.A. Simulation of catalytic reduction of nitrates based on a mechanistic model. *Chemical engineering journal* **2011**, *175*, 458-467.
42. Paavani, K.; Agarwal, K.; Alam, S.S.; Dinda, S.; Abrar, I. Advances in plastic to fuel conversion: reactor design, operational optimization, and machine learning integration. *Sustainable Energy & Fuels* **2025**, *9*, 54-71.
43. Benavides-Hernández, J.; Dumeignil, F. From Characterization to Discovery: Artificial Intelligence, Machine Learning and High-Throughput Experiments for Heterogeneous Catalyst Design. *ACS Catalysis* **2024**, *14*, 11749-11779.
44. He, C.; Xie, K.; Lin, L.; Huo, J.; Zhao, C.; Li, L. Efficient Electrocatalytic N2fixation Over Bc3n2monolayer: A Computational Screening of Single-Atom Catalysts. *Available at SSRN 4066356*.
45. Zhang, K.; Zou, X.; Liu, Y.; Zhang, X.; An, L. Progress and Perspectives in Electroreduction of Low-concentration Nitrate for Wastewater Management. *iScience* **2024**.
46. Miller, D.M.; Liu, M.J.; Abels, K.; Kogler, A.; Williams, K.S.; Tarpeh, W.A. Engineering a molecular electrocatalytic system for energy-efficient ammonia production from wastewater nitrate. *Energy & Environmental Science* **2024**, *17*, 5691-5705.
47. Barrera, L.; Bala Chandran, R. Harnessing photoelectrochemistry for wastewater nitrate treatment coupled with resource recovery. *ACS Sustainable Chemistry & Engineering* **2021**, *9*, 3688-3701.
48. Tyagi, V.K.; Kumar, M.; An, A.K.; Cetecioglu, Z. Clean energy and resource recovery: wastewater treatment plants as biorefineries, Volume 2; Elsevier: 2021.
49. Zhang, H.; Yu, Z.; Wang, J.; Ke, Z.; Tong, L.; Tang, X.; Bai, L.; Zhang, H.; Li, G.; Liang, H. A review of inland nanofiltration and reverse osmosis membrane concentrates management: Treatment, resource recovery and future development. *Critical Reviews in Environmental Science and Technology* **2024**, 1-27.
50. Feng, Y.; Ren, J.-T.; Sun, M.-L.; Yuan, Z.-Y. Valorization systems based on electrocatalytic nitrate/nitrite conversion for energy supply and valuable product synthesis. *Chemical Science* **2025**.
51. Li, L.; Xu, L.; Wang, H.; Wei, H.; Tang, C.; Li, G.; Dou, Y.; Liu, H.; Dou, S.X. Electrocatalytic nitrogen cycle: mechanism, materials, and momentum. *Energy & Environmental Science* **2024**.
52. Wani, N.R.; Rather, R.A.; Farooq, A.; Padder, S.A.; Baba, T.R.; Sharma, S.; Mubarak, N.M.; Khan, A.H.; Singh, P.; Ara, S. New insights in food security and environmental sustainability through waste food management. *Environmental Science and Pollution Research* **2024**, *31*, 17835-17857.

53. Fernandez, C.A.; Chapman, O.; Brown, M.A.; Alvarez-Pugliese, C.E.; Hatzell, M.C. Achieving Decentralized, Electrified, and Decarbonized Ammonia Production. *Environmental Science & Technology* **2024**, *58*, 6964-6977.
54. Sun, S.; Dai, C.; Zhao, P.; Xi, S.; Ren, Y.; Tan, H.R.; Lim, P.C.; Lin, M.; Diao, C.; Zhang, D. Spin-related Cu-Co pair to increase electrochemical ammonia generation on high-entropy oxides. *Nature Communications* **2024**, *15*, 260.
55. Huang, W.; Luo, W.; Liu, J.; Jia, B.E.; Lee, C.; Dong, J.; Yang, L.; Liu, B.; Yan, Q. Cascade Electrocatalytic Nitrate Reduction Reaching 100% Nitrate-N to Ammonia-N Conversion over Cu(2)O@CoO Yolk-Shell Nanocubes. *ACS Nano* **2024**, doi:10.1021/acsnano.4c03995.
56. Habib, U.; Ahmad, F.; Awais, M.; Naz, N.; Aslam, M.; Urooj, M.; Moqeem, A.; Tahseen, H.; Waqar, A.; Sajid, M. Sustainable Catalysis: Navigating Challenges and Embracing Opportunities for a Greener Future. *Journal of Chemistry and Environment* **2023**, *2*, 14-53.
57. Sekhar, S.J.; Al-Shahri, A.S.A.; Glivin, G.; Le, T.; Mathimani, T. A critical review of the state-of-the-art green ammonia production technologies-mechanism, advancement, challenges, and future potential. *Fuel* **2024**, *358*, 130307.
58. Shu, Y.; Wang, D.; Wang, J.; Huang, H. Adsorption and photocatalytic degradation of Ammonia: Status and challenges. *Chemical Engineering Journal* **2024**, 154925.
59. Rafiqul Bari, G.A.; Jeong, J.-H. Comprehensive Insight and Advancements in Material Design for Electrocatalytic Ammonia Production Technologies: An Alternative Clean Energy. *International Journal of Energy Research* **2024**, *2024*, 5685619.
60. Din, I.U.; Nasir, Q.; Garba, M.D.; Alharthi, A.I.; Alotaibi, M.A.; Usman, M. A review of preparation methods for heterogeneous catalysts. *Mini-Reviews in Organic Chemistry* **2022**, *19*, 92-110.
61. Li, H.; Li, R.; Liu, G.; Zhai, M.; Yu, J. Noble-metal-free single-and dual-atom catalysts for artificial photosynthesis. *Advanced Materials* **2024**, *36*, 2301307.
62. Campbell, E.; Brown, A.; Nguyen, H.T.M.; He, K.; Batmunkh, M.; Zhong, Y.L. Recent Advances in Selective Chemical Etching of Nanomaterials for High-Performance Electrodes in Electrocatalysis and Energy Storage. *Small* **2024**, 2409552.
63. Ma, Z.; Wang, C.; Yang, T.; Wei, G.; Huang, J.; Liu, M.; Zhang, K.; Zhang, Z.; Liu, Y.; Gao, S. A 3D porous P-doped Cu–Ni alloy for atomic H* enhanced electrocatalytic reduction of nitrate to ammonia. *Journal of Materials Chemistry A* **2024**, *12*, 7654-7662.
64. Lv, S.; Gou, F.; Wang, H.; Jiang, Y.; Shen, W.; He, R.; Li, M. Interface coupling of Ni2P@ Cu3P catalyst to facilitate highly-efficient electrochemical reduction of nitrate to ammonia. *Applied Surface Science* **2024**, *648*, 159082.
65. Jin, M.; Liu, J.; Zhang, X.; Zhang, S.; Li, W.; Sun, D.; Zhang, Y.; Wang, G.; Zhang, H. Heterostructure Cu3P–Ni2P/CP catalyst assembled membrane electrode for high-efficiency electrocatalytic nitrate to ammonia. *Nano Research* **2024**, 1-10.
66. Min, L.; Liping, S.; Lihua, H.; Hui, Z. Highly efficient electrolytic reduction of nitrate to produce ammonia using Cu@ Ni2P-NF Schottky heterojunction. *Applied Catalysis A: General* **2024**, *676*, 119650.
67. Li, S.; Han, D.; Jiang, G.; Han, Z.; Lu, H.; Gao, J.; Wang, X.; Wang, Y.; Geng, C.; Weng, Z. Proton Exchange Membrane Electrode Assembly for Ammonia Electrosynthesis from Nitrate. *ACS Applied Energy Materials* **2023**, *6*, 5067-5073.
68. Zhang, L.H.; Jia, Y.; Zhan, J.; Liu, G.; Liu, G.; Li, F.; Yu, F. Dopant-Induced Electronic States Regulation Boosting Electroreduction of Dilute Nitrate to Ammonium. *Angewandte Chemie International Edition* **2023**, *62*, e202303483.
69. Gong, Z.; Xiang, X.; Zhong, W.; Jia, C.; Chen, P.; Zhang, N.; Zhao, S.; Liu, W.; Chen, Y.; Lin, Z. Modulating Metal-Nitrogen Coupling in Anti-Perovskite Nitride via Cation Doping for Efficient Reduction of Nitrate to Ammonia. *Angewandte Chemie* **2023**, *135*, e202308775.
70. Zhang, S.; Li, M.; Li, J.; Song, Q.; Liu, X. High-ammonia selective metal–organic framework–derived Co-doped Fe/Fe2O3 catalysts for electrochemical nitrate reduction. *Proceedings of the National Academy of Sciences* **2022**, *119*, e2115504119.

71. Zhang, R.; Guo, Y.; Zhang, S.; Chen, D.; Zhao, Y.; Huang, Z.; Ma, L.; Li, P.; Yang, Q.; Liang, G. Efficient ammonia electrosynthesis and energy conversion through a Zn-nitrate battery by iron doping engineered nickel phosphide catalyst. *Advanced Energy Materials* **2022**, *12*, 2103872.
72. Zhao, Y.; Shen, J.; Yuan, J.; Mao, H.; Cheng, X.; Xu, Z.; Bian, Z. Modulating electronic structures of MOF through orbital rehybridization by Cu doping promotes photocatalytic reduction of nitrate to produce ammonia. *Nano Energy* **2024**, 109499.
73. Lim, J.; Chen, Y.; Cullen, D.A.; Lee, S.W.; Senftle, T.P.; Hatzell, M.C. PdCu electrocatalysts for selective nitrate and nitrite reduction to nitrogen. *ACS Catalysis* **2022**, *13*, 87-98.
74. Li, R.; Gao, T.; Wang, P.; Qiu, W.; Liu, K.; Liu, Y.; Jin, Z.; Li, P. The origin of selective nitrate-to-ammonia electroreduction on metal-free nitrogen-doped carbon aerogel catalysts. *Applied Catalysis B: Environmental* **2023**, *331*, 122677.
75. Yin, H.; Chen, Z.; Xiong, S.; Chen, J.; Wang, C.; Wang, R.; Kuwahara, Y.; Luo, J.; Yamashita, H.; Peng, Y. Alloying effect-induced electron polarization drives nitrate electroreduction to ammonia. *Chem Catalysis* **2021**, *1*, 1088-1103.
76. Cai, J.; Wei, Y.; Cao, A.; Huang, J.; Jiang, Z.; Lu, S.; Zang, S.-Q. Electrocatalytic nitrate-to-ammonia conversion with~ 100% Faradaic efficiency via single-atom alloying. *Applied Catalysis B: Environmental* **2022**, *316*, 121683.
77. Lim, J.; Cullen, D.A.; Stavitski, E.; Lee, S.W.; Hatzell, M.C. Atomically ordered PdCu electrocatalysts for selective and stable electrochemical nitrate reduction. *ACS Energy Letters* **2023**, *8*, 4746-4752.
78. Wang, Y.; Xu, A.; Wang, Z.; Huang, L.; Li, J.; Li, F.; Wicks, J.; Luo, M.; Nam, D.-H.; Tan, C.-S. Enhanced nitrate-to-ammonia activity on copper–nickel alloys via tuning of intermediate adsorption. *Journal of the American Chemical Society* **2020**, *142*, 5702-5708.
79. Gao, W.; Xie, K.; Xie, J.; Wang, X.; Zhang, H.; Chen, S.; Wang, H.; Li, Z.; Li, C. Alloying of Cu with Ru enabling the relay catalysis for reduction of nitrate to ammonia. *Advanced Materials* **2023**, *35*, 2202952.
80. Zhao, Z.; Zhang, X.; Liu, X.; Li, B.; Ren, Z.; Zhu, X.; Liu, X.; O'Mullane, A.P. Preparation of a branched hierarchical Co3O4@ Fe2O3 core–shell structure with high-density catalytic sites for efficient catalytic conversion of nitrate in wastewater to ammonia. *Chemical Engineering Journal* **2024**, *499*, 156495.
81. Zhang, Y.; Gao, T.; Zhang, F.; Qu, X.; Luo, Y.; Zhang, P.; Liang, J.; Song, Y.; Fang, F.; Wang, F. Regioselective Doping into Atomically Aligned Core–Shell Structures for Electrocatalytic Reduction of Nitrate to Ammonia. *Advanced Energy Materials* **2024**, 2401834.
82. Gao, Q.; Yao, B.; Pillai, H.S.; Zang, W.; Han, X.; Liu, Y.; Yu, S.-W.; Yan, Z.; Min, B.; Zhang, S. Synthesis of core/shell nanocrystals with ordered intermetallic single-atom alloy layers for nitrate electroreduction to ammonia. *Nature Synthesis* **2023**, *2*, 624-634.
83. Shi, X.; Xie, M.; Yang, K.; Niu, Y.; Ma, H.; Zhu, Y.; Li, J.; Pan, T.; Zhou, X.; Cui, Y. Synergistic Effect of Ni/Ni (OH) 2 Core-Shell Catalyst Boosts Tandem Nitrate Reduction for Ampere-Level Ammonia Production. *Angewandte Chemie* **2024**, e202406750.
84. Bielan, Z.; Sulowska, A.; Dudziak, S.; Siuzdak, K.; Ryl, J.; Zielińska-Jurek, A. Defective TiO2 core-shell magnetic photocatalyst modified with plasmonic nanoparticles for visible light-induced photocatalytic activity. *Catalysts* **2020**, *10*, 672.
85. Wang, M.; Wei, G.; Li, R.; Yu, M.; Liu, G.; Peng, Y. Schottky Junctions with Bi@ Bi2MoO6 Core-Shell Photocatalysts toward High-Efficiency Solar N2-to-Ammonnia Conversion in Aqueous Phase. *Nanomaterials* **2024**, *14*, 780.
86. Melnikov, D.; Smirnova, E.; Reshetina, M.; Novikov, A.; Wang, H.; Ivanov, E.; Vinokurov, V.; Glotov, A. Mesoporous Chromium Catalysts Templated on Halloysite Nanotubes and Aluminosilicate Core/Shell Composites for Oxidative Dehydrogenation of Propane with CO2. *Catalysts* **2023**, *13*, 882.
87. Xu, J.; Yang, Z.; Chen, S.; Wang, W.; Zhang, Y. Compatibility and Photocatalytic Capacity of the Novel Core@ shell Nanospheres in Cementitious Composites. *Catalysts* **2022**, *12*, 1574.
88. Suh, J.; Choi, H.; Kong, Y.; Oh, J. Tandem Electroreduction of Nitrate to Ammonia Using a Cobalt-Copper Mixed Single-Atom/Cluster Catalyst with Synergistic Effects. *Adv Sci (Weinh)* **2024**, e2407250, doi:10.1002/advs.202407250.

89. Mehmood, S.; Sk, S.; Abraham, B.M.; Ahmadipour, M.; Pal, U.; Dutta, J. Recent Advances in Single-Atom Catalyst for Solar Energy Conversion: A Comprehensive Review and Future Outlook. *Advanced Functional Materials*, 2418602.
90. Li, Z.; Hong, R.; Zhang, Z.; Wang, H.; Wu, X.; Wu, Z. Single-atom catalysts in environmental engineering: Progress, outlook and challenges. *Molecules* **2023**, *28*, 3865.
91. Zhao, K.; Wang, J.; Yang, Y.; Wang, X. Efficient Electrocatalytic Ammonia Synthesis via Theoretical Screening of Titanate Nanosheet-Supported Single-Atom Catalysts. *Materials* **2024**, *17*, 2239.
92. Fang, J.-Y.; Fan, J.-L.; Liu, S.-B.; Sun, S.-P.; Lou, Y.-Y. Copper-based electrocatalysts for nitrate reduction to ammonia. *Materials* **2023**, *16*, 4000.
93. Chi, X.; Cang, Y.; Wang, J.; Li, Q.; Fan, X.; Lin, H. Electrocatalytic N2 Reduction Driven by Mo-Based Double-Atom Catalysts Anchored on Graphdiyne. *Catalysts* **2024**, *14*, 879.
94. Shen, Z.; Yu, Y.; Zhao, Z.; Mushtaq, M.A.; Ji, Q.; Yasin, G.; Rehman, L.N.U.; Liu, X.; Cai, X.; Tsiakaras, P. N, O trans-coordinating silver single-atom catalyst for robust and efficient ammonia electrosynthesis from nitrate. *Applied Catalysis B: Environmental* **2023**, *331*, 122687.
95. Song, W.; Yue, L.; Fan, X.; Luo, Y.; Ying, B.; Sun, S.; Zheng, D.; Liu, Q.; Hamdy, M.S.; Sun, X. Recent progress and strategies on the design of catalysts for electrochemical ammonia synthesis from nitrate reduction. *Inorganic Chemistry Frontiers* **2023**, *10*, 3489-3514.
96. Yin, S.; Guan, Z.; Zhu, Y.; Guo, D.; Chen, X.a.; Wang, S. Highly Efficient Electrocatalytic Nitrate Reduction to Ammonia: Group VIII-Based Catalysts. *ACS nano* **2024**, *18*, 27833-27852.
97. Vieri, H.M.; Kim, M.-C.; Badakhsh, A.; Choi, S.H. Electrochemical Synthesis of Ammonia via Nitrogen Reduction and Oxygen Evolution Reactions—A Comprehensive Review on Electrolyte-Supported Cells. *Energies* **2024**, *17*, 441.
98. Gao, W.; Perales-Rondon, J.V.; Michalička, J.; Pumera, M. Ultrathin manganese oxides enhance the electrocatalytic properties of 3D printed carbon catalysts for electrochemical nitrate reduction to ammonia. *Applied Catalysis B: Environmental* **2023**, *330*, 122632.
99. Hao, J.; Wang, T.; Yu, R.; Cai, J.; Gao, G.; Zhuang, Z.; Kang, Q.; Lu, S.; Liu, Z.; Wu, J. Integrating few-atom layer metal on high-entropy alloys to catalyze nitrate reduction in tandem. *Nature Communications* **2024**, *15*, 9020.
100. Guo, W.; Zhao, T.; Li, F.; Cai, Q.; Zhao, J. Si3C monolayer as an efficient metal-free catalyst for nitrate electrochemical reduction: a computational study. *Nanomaterials* **2023**, *13*, 2890.
101. Han, C.; Li, C.; Yuwono, J.A.; Liu, Z.; Sun, K.; Wang, K.; He, G.; Huang, J.; Kumar, P.V.; Vongsvivut, J. Nanostructured hybrid catalysts empower the artificial leaf for solar-driven ammonia production from nitrate. *Energy & Environmental Science* **2024**, *17*, 5653-5665.
102. Padinjareveetil, A.K.K.; Perales-Rondon, J.V.; Pumera, M. Engineering 3D printed structures towards electrochemically driven green ammonia synthesis: a perspective. *Advanced Materials Technologies* **2023**, *8*, 2202080.
103. Zhao, N.; Wang, J.; Song, S.; Li, C.; Wang, J.; Li, X.; Pan, Z.; Yuan, J.; Zhu, L.; Pan, M. Convenient hydrothermal treatment combining with "Ship in Bottle" to construct Yolk-Shell N-Carbon@ Ag-void@ mSiO2 for high effective Nano-Catalysts. *Applied Surface Science* **2023**, *624*, 157158.
104. He, H.; Wen, H.-M.; Li, P.; Li, H.-K.; Li, C.-P.; Zhang, Z.; Du, M. Tailor-made yolk-shell nanocomposites of star-shape Au and porous organic polymer for nitrogen electroreduction to ammonia. *Chemical Engineering Journal* **2023**, *476*, 146760.
105. Li, Z.; Li, B.; Yu, C.; Wang, H.; Li, Q. Recent progress of hollow carbon nanocages: general design fundamentals and diversified electrochemical applications. *Advanced Science* **2023**, *10*, 2206605.
106. Zhang, Y.; Xiong, J.; Wang, X.; Li, M.; Yan, S.; Liu, B. Zif-Derived Cos@ Cn with a Hollow Cage Structure for Improved Electrochemical Nitrate Reduction to Synthesize Ammonia. *Available at SSRN 5008941*.
107. Yuan, X.-Z.; Shaigan, N.; Song, C.; Aujla, M.; Neburchilov, V.; Kwan, J.T.H.; Wilkinson, D.P.; Bazylak, A.; Fatih, K. The porous transport layer in proton exchange membrane water electrolysis: perspectives on a complex component. *Sustainable Energy & Fuels* **2022**, *6*, 1824-1853, doi:10.1039/d2se00260d.
108. Sun, J.W.; Fu, H.Q.; Liu, P.F.; Chen, A.; Liu, P.; Yang, H.G.; Zhao, H. Advances and challenges in scalable carbon dioxide electrolysis. *EES Catalysis* **2023**, *1*, 934-949, doi:10.1039/d3ey00159h.

109. Chen, F.-Y.; Elgazzar, A.; Pecaut, S.; Qiu, C.; Feng, Y.; Ashokkumar, S.; Yu, Z.; Sellers, C.; Hao, S.; Zhu, P.; et al. Electrochemical nitrate reduction to ammonia with cation shuttling in a solid electrolyte reactor. *Nature Catalysis* **2024**, *7*, 1032-1043, doi:10.1038/s41929-024-01200-w.
110. Jin, M.; Liu, J.; Zhang, X.; Zhang, S.; Li, W.; Sun, D.; Zhang, Y.; Wang, G.; Zhang, H. Heterostructure Cu3P−Ni2P/CP catalyst assembled membrane electrode for high-efficiency electrocatalytic nitrate to ammonia. *Nano Research* **2024**, *17*, 4872-4881, doi:10.1007/s12274-024-6474-z.
111. Zhu, H.; Wang, J.J.; Xu, Z.; Tan, Y.; Wang, J. Pd Nanoparticle Size-Dependent H(*) Coverage for Cu-Catalyzed Nitrate Electro-Reduction to Ammonia in Neutral Electrolyte. *Small* **2024**, e2404919, doi:10.1002/smll.202404919.
112. Zhang, X.; Liu, X.; Huang, Z.-F.; Guo, L.; Gan, L.; Zhang, S.; Ajmal, M.; Pan, L.; Shi, C.; Zhang, X.; et al. Tandem Nitrate Electroreduction to Ammonia with Industrial-Level Current Density on Hierarchical Cu Nanowires Shelled with NiCo-Layered Double Hydroxide. *ACS Catalysis* **2023**, *13*, 14670-14679, doi:10.1021/acscatal.3c04541.
113. Qian, Y.; Lv, J.; Zhong, Y.; Liu, X.; Li, X.; Peng, Y.; Yan, J.; Wu, A. Efficient electrocatalytic nitrate reduction using 3D copper foam-supported Co hexagonal nanoparticles in a membrane electrode assembly. *International Journal of Hydrogen Energy* **2024**, *64*, 178-185, doi:10.1016/j.ijhydene.2024.03.119.
114. Huang, P.W.; Song, H.; Yoo, J.; Chipoco Haro, D.A.; Lee, H.M.; Medford, A.J.; Hatzell, M.C. Impact of Local Microenvironments on the Selectivity of Electrocatalytic Nitrate Reduction in a BPM-MEA System. *Advanced Energy Materials* **2024**, *14*, doi:10.1002/aenm.202304202.
115. Guo, Y.; Tong, Y.; Zhou, G.; He, J.; Ren, X.; Chen, L.; Chen, P. Oxygen-deficient NiCo2O4 porous nanowire for superior electrosynthesis of ammonia coupling with valorization of ethylene glycol. *Chemical Engineering Journal* **2024**, *496*, doi:10.1016/j.cej.2024.154220.
116. Li, S.; Han, D.; Jiang, G.; Han, Z.; Lu, H.; Gao, J.; Wang, X.; Wang, Y.; Geng, C.; Weng, Z.; et al. Proton Exchange Membrane Electrode Assembly for Ammonia Electrosynthesis from Nitrate. *ACS Applied Energy Materials* **2023**, *6*, 5067-5073, doi:10.1021/acsaem.3c00709.
117. Gan, L.; Zhang, X.; Guo, L.; Ajmal, M.; Jia, R.; Guo, X.; Shi, C.; Pan, L.; Idrees, F.; Zhang, X.; et al. Redirecting surface reconstruction of CoP-Cu heterojunction to promote ammonia synthesis at industrial-level current density. *Chemical Engineering Journal* **2024**, *487*, doi:10.1016/j.cej.2024.150429.
118. Yuan, T.; Li, M.; Subramanian, S.; Kok, J.; Li, M.; Urakawa, A.; Voznyy, O.; Burdyny, T. Sequential electrocatalytic reactions along a membrane electrode assembly drive efficient nitrate-to-ammonia conversion. *Cell Reports Physical Science* **2024**, *5*, doi:10.1016/j.xcrp.2024.101977.